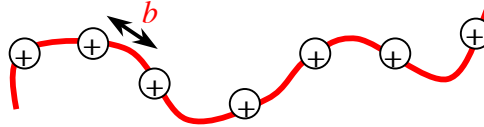


II. Charged Polymer Systems – Electrostatic and Conformational Descriptions

Polyelectrolytes

Electrostatic Description –



The simplest description of a polyelectrolyte imagines, as sketched above, discrete fixed charges positioned at an average axial spacing b along a backbone of infinitesimal thickness.

Electrostatic interactions among the fixed charges are modulated by the solvent dielectric constant ϵ , and a dimensionless parameter ξ captures the strength of interaction with a neighboring charge relative to the ambient thermal energy kT ,

$$\xi = \frac{l_b}{b} = \frac{e^2}{4\pi\epsilon\epsilon_0 kTb}$$

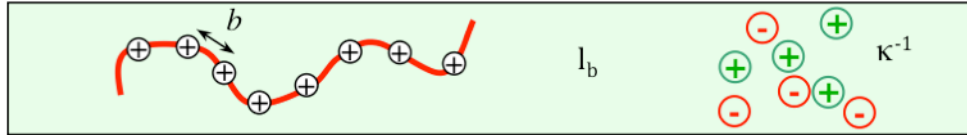
Within the chosen physical description – a curvilinear collection of ionizable units that dissociate free ions to infinity - the dependences of all polyelectrolyte properties on ϵ , T , and b are collapsed into a single dependence on ξ .

The parameter ξ , often called the Manning parameter, fundamentally distinguishes a charged polymer system from a neutral one or one charged polymer system from another.

When $\xi < 1$, electrostatic forces acting on the chain at the length scale of the charge spacing are always weak compared to thermal fluctuations, defining a “weakly charged” polyelectrolyte as one that behaves much as a neutral polymer. Nonetheless, such a polymer will show polyelectrolyte properties, especially in its interactions with other charged molecules. When $\xi \geq 1$, electrostatic forces locally dominate over thermal fluctuations, and the term “strongly charged” polyelectrolyte is employed. For the latter, behaviors distinct from a neutral polymer are expected if the level of added electrolyte is not so high as to screen fully all electrostatic interactions among the backbone charges.

Water is the most important dielectric medium, and l_b for water is 7.1 \AA at room temperature, a dimension larger than the repeat unit length (or diameter) of most synthetic polymers as well as the hydrated sizes of many dissolved ions. For the charged polymers illustrated in the last handout range, $0 < \xi < 5$. Even larger values of ξ are obtained for “bottlebrush” polyelectrolytes, i.e., those with multiple ionizable units on side chains attached to the polymer backbone. The most highly charged biopolymer is heparin.

In the simplest electrostatic description of a polyelectrolyte system, the medium contributes one length scale (l_b), the polymer contributes a second (b), and the electrolyte (dissociated small ions and any added salt) contributes a third (κ^{-1}). Missing from this description are diameters of polyelectrolyte and dissociated ions, correlations in position among dissociated ions, the discrete molecular nature of the solvent, and the local geometry and dielectric constant of the chain itself.

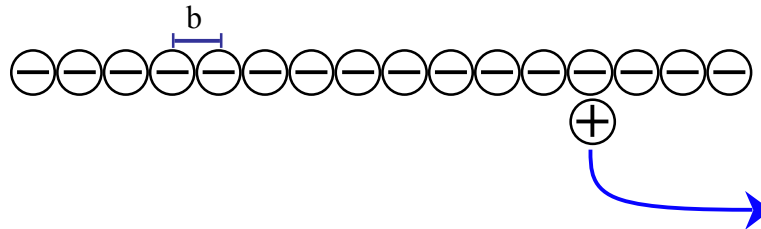


Electrostatic forces in an electrolyte reach over a longest length scale of several κ^{-1} and are significant over the dimensions typical of polymer segments and l_b , not those of polymer coils. Thus, characteristic polyelectrolyte behaviors - those distinct to this class of polymers - are all local in origin and independent of parameters such as chain length or coil size. Characteristic behaviors propagate to larger polymer lengths scales, affecting polymer coil properties, but they don't create any new effects in doing so. We thus can understand fundamental polyelectrolyte principles by analyzing electrostatics at the segmental size scale.

Counterion Condensation –

In a variety of contexts, highly charged polyelectrolytes behave as if their net charge, or more precisely, their effective linear charge density, is less than the one calculated from the linear density of ionizable units in the chain's chemical structure. For example, at physiological pH, ds-DNA has often been reported to display an “effective” charge ~75% less than expected by the dissociation of two phosphates per base pair. Given the large dissociation constants of phosphate, these groups are expected to ionize essentially fully at neutral pH.

To understand the apparent charge reduction, consider the dissociation of the “last” ionizable unit of an infinitely long, strong polyelectrolyte, perhaps extended, as shown below, at the segmental level due to strong repulsions between previously ionized units.



The energy for this dissociation in a dielectric medium, described in the last handout, can be written as a sum of all pairwise electrostatic interactions between chain and dissociated ion.

$$\frac{U}{kT} = 2 \left(\frac{e^2}{4\pi\epsilon\epsilon_0 kT} \right) \sum_{j=1}^{\infty} \frac{1}{r_j} = \frac{e^2}{2\pi\epsilon\epsilon_0 kT} \sum_{j=1}^{\infty} \frac{1}{bj} = 2\xi \sum_{j=1}^{\infty} \frac{1}{j} = \infty$$

The index j corresponds to interactions of the targeted unit ($j=0$) with already ionized units extending in both directions along the backbone, explaining the multiplicative factor and 2, and j can be considered to reach ∞ since pairwise electrostatic interactions lose their strength long before j reaches its largest value at the chain ends. The apparent singularity in U/kt highlights the overwhelming impact of collective electrostatic on polyelectrolyte dissociation. The entropy gained by the counterion's release, of order kT , cannot overcome the enthalpy associated with electrostatic attraction to the chain. According to this calculation, the dissociated counterion must remain “clustered” or “condensed” near the polymer backbone, effectively neutralizing some backbone charge. It is important to note

that these condensed counterions are truly dissociated, the concern is their locations relative to the backbone after dissociation.

The hypothesized “condensation” of oppositely charged small ions reduce the polyelectrolyte’s “apparent” or “effective” charge even when the chain’s ionizable units are known to dissociate at the bulk solution condition. This binding of condensed counterions arises from electrostatic forces within the solution phase, not from specific interactions of ions with the polyelectrolyte; in other words, the dissociation constant of the ionizable units is unimportant.

The preceding calculation can be repeated using the electrostatic energy appropriate to an electrolyte medium of Debye length κ^{-1} ,

$$\frac{U}{KT} = 2 \left(\frac{e^2}{4\pi\epsilon\epsilon_0 kT} \right) \sum_{j=1}^{\infty} \frac{e^{-\kappa r_j}}{r_j} = 2\xi \sum_{j=1}^{\infty} \frac{e^{-\kappa b j}}{j} = -2\xi \ln(1 - e^{-\kappa b}) \approx -2\xi \ln \kappa b$$

a result also reached by evaluating the electrostatic energy of a counterion in the potential field of a line charge (this potential was given in the last handout).

While the dissociation energy is no longer singular, it still diverges in the limit of small κb , i.e., at low or no added electrolyte, a nonsensical result.

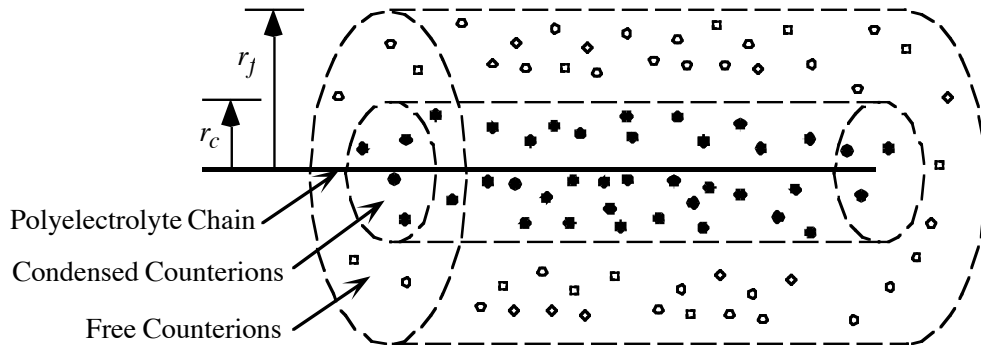
The traditional resolution to this paradox is “counterion condensation”, the formal splitting of the dissociated counterion population into two states, those “condensed” against the chain backbone and those “free” to sample the surrounding solvent.

Oosawa (1968) and Manning (1969) independently formalized the counterion condensation concept at about the same time. Manning subsequently clarified and extended the proposition to such a degree that the phenomenon is now frequently referenced simply as “Manning condensation.” Actually, Imai and Onishi coined the term “counterion condensation” in 1959, and reference to the strong clustering of a portion of counterions at low salt solutions goes back to Fuoss in the 1949.

In its simplest form, counterion condensation minimizes the free energy of small counterions located near a polyelectrolyte chain, incorporating both entropic and electrostatic energy contributions in the minimization. In most models, as sketched on the next page, the chain is represented as an infinite line or a thin, infinite cylinder. Unfortunately, these geometric descriptions obscure the extrapolation of theoretical predictions to flexible polyelectrolytes. The fixed charges may be treated as either “smeared” along the backbone or “fixed” at discrete axial positions; these treatments of charge location produce nearly identical results.

Counterions released into solvent from a single, isolated polyelectrolyte sample an enlarged region of space, and therefore their contributions to system entropy rise upon their release. However, the entropy enhancement comes at a cost, as the further into outlying space the counterions explore, the greater is their electrostatic energy. Condensed ions possess freedom only to move along and near the chain backbone while free ions move in a more or less unconstrained fashion throughout the solvent domain away from the backbone. The

following figure provides a schematic of the postulated counterion populations near a line charge.



Issues key to counterion condensation are the fraction of free ions and the extent to which the condensed ions are localized. [Exchange of counterions between condensed and free populations is an interesting but not central question. Condensed ions should not be viewed in the same way that separated gas molecules combined to form a liquid; the terminology “condensed” is unfortunate.]

Some authors define two subpopulations of condensed ions: “site bound” condensed ions are those in direct contact with the polyelectrolyte (no intervening water molecules) and “territorially bound” condensed ions are those nonspecifically attached to the polyelectrolyte backbone, probably with their primary solvation layer intact. Only territorially bound condensed ions are able to wander readily along the chain’s contour.

Oosawa Argument for Counterion Condensation

Oosawa argued that the concentrations of condensed and free counterions are related by an appropriate Boltzmann factor,

$$n_c = n_f \exp\left[\frac{-e\Delta\psi}{kT}\right] \quad (1)$$

where $\Delta\psi$ is the potential difference between the outer edge of the annular region containing free ions (see Figure 1) and the outer edge of cylindrical core region containing condensed ions; electrostatic potentials across both regions are assumed constant, as are their respective counterion volume densities n_c and n_f . If β is the fraction of dissociated counterions that are free, the polyelectrolyte’s effective charge density ξ_{eff} (summing the charge of the core region, including both ionized polyelectrolyte AND condensed counterions) is given $\beta\xi$.

As quickly derived from a result in the previous handout, in a dielectric medium the electrostatic potential near an infinitely long, isolated line charge decays logarithmically with radial distance r ,

$$\psi = -2\xi\left(\frac{kT}{e}\right)\ln r$$

Letting the outer radius of the condensed ion region be denoted r_c and the outer radius of the free ion region be denoted r_f , $\Delta\psi$ can be estimated,

$$\Delta\psi = -2\xi_{\text{eff}} \left(\frac{kT}{e} \right) \ln \left(\frac{r_f}{r_c} \right) = -\xi_{\text{eff}} \left(\frac{kT}{e} \right) \ln \left(\frac{V_f + V_c}{V_c} \right) \quad (2)$$

where V_c and V_f are volumes of the condensed and free ion regions, respectively.

Equations 1 and 2 can be combined to eliminate $\Delta\psi$,

$$\ln \frac{n_c}{n_f} = -\frac{e\Delta\psi}{kT} = \xi_{\text{eff}} \ln \left(\frac{V_f + V_c}{V_c} \right) = \beta\xi \ln \left(\frac{V_f + V_c}{V_c} \right) \quad (3)$$

Counting the condensed and free ions by taking the respective products $n_c V_c$ and $n_f V_f$,

$$\ln \left(\frac{1-\beta}{\beta} \right) = \ln \left(\frac{n_c V_c}{n_f V_f} \right) = \ln \frac{n_c}{n_f} + \ln \frac{V_c}{V_f} \quad (4)$$

Designating ϕ as the fraction of space containing condensed ions [i.e., $\phi = V_c/(V_c + V_f)$], the two previous equations can be combined in a final expression relating ϕ and β ,

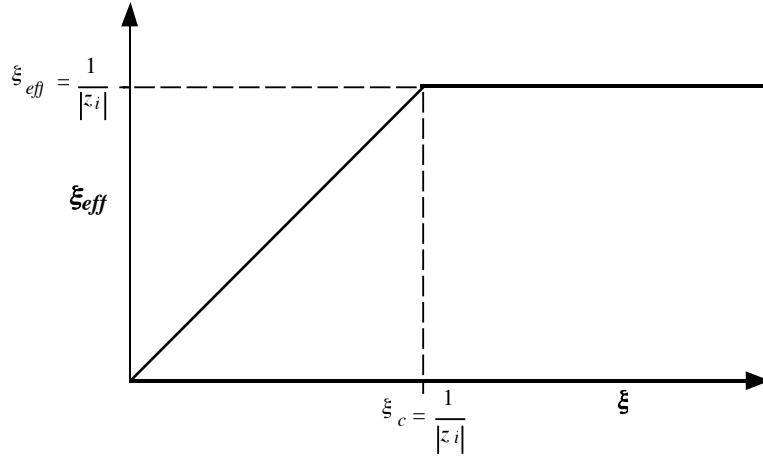
$$\ln \frac{1-\beta}{\beta} = \ln \frac{\phi}{1-\phi} - \beta\xi \ln \phi \quad (5)$$

In the limit $\phi \rightarrow 0$, V_c becomes exceedingly small, and Oosawa demonstrated for the preceding expression the existence of two solution types. When $\xi \leq 1$, a solution exists for $\beta \rightarrow 1$, and when $\xi > 1$, a solution exists for $\beta = 1/\xi$. The second solution reveals condensed counterions when a polyelectrolyte is highly charged. Further, it shows that $\xi_{\text{eff}} = 1$ for $\xi > 1$, i.e., sufficiently many counterions condense so as to maintain a fixed effective charge density, i.e., one that does not depend on the actual density of dissociated ionizable units.

The condition $\xi_c = 1$ is viewed as the critical condition for the onset of counterion condensation for monovalent counterions.

With these results in hand, the statement about DNA that opened this section is readily interpreted. For this polymer, $\xi \approx 4.2$. If $\xi_{\text{eff}} = 1$ for $\xi > 1$, then $\sim 75\%$ ($3.2/4.2$) of the charge from dissociated phosphates is compensated by condensed counterions.

The same trends apply to higher valence counterions except that the onset of counterion condensation is lowered to $\xi_c = |z_i|^{-1}$, and for $\xi > \xi_c$, $\beta = 1/|z_i|\xi$. The next figure sketches these predictions.



Manning Argument for Counterion Condensation

Manning's proposed arguments for counterion condensation superior to the one presented above. His arguments allow ψ in the region occupied by free ions to be electrostatically screened at the level of the Debye-Hückel approximation.

The Debye-Hückel electrostatic potential near a line charge was given in the last handout, and after being rewritten in terms of ξ , it reads,

$$\psi(r) = 2\xi \left(\frac{kT}{e} \right) K_0(r\kappa) \quad (6)$$

Manning calculated the radial charge distribution by asserting Boltzmann distributions for the co- and counter-ions residing in this screened potential. For 1:1 electrolyte,

$$\rho(r) = n_b e [\underbrace{\exp(-e\psi / kT)}_{\text{co-ions}} - \underbrace{\exp(e\psi / kT)}_{\text{counterions}}] \quad (7)$$

where n_b is the bulk volume density of coion and counterion.

From the charge distribution, the excess of charge residing inside a surface of radius r is given by the integral,

$$Q(r) = \int_0^r \rho(r) (2\pi r) dr \quad (8)$$

Near the hypothesized line charge (small $r\kappa$), the following approximation holds (see any math handbook),

$$K_0(r\kappa) = 0.1159 - \ln(r\kappa) + \dots \quad (9)$$

Applying this approximation to the preceding integral and then rearranging,

$$Q(r) = 2\pi n_b e \left[\underbrace{\exp(-0.23\xi) \int_0^r (\kappa r)^{2\xi} r dr}_{\text{co-ions}} - \underbrace{\exp(0.23\xi) \int_0^r (\kappa r)^{-2\xi} r dr}_{\text{counterions}} \right] \quad (10)$$

The first integral is well behaved. However, neglecting its multiplicative prefactor, the second integral yields

$$\frac{r^{2(1-\xi)}}{2(1-\xi)\kappa^{2\xi}} \Big|_0^r \quad (11)$$

which diverges unless $\xi < 1$. Seeing this behavior, Manning wrote the following (with minor changes to bring his vocabulary in line with this handout), “The physical interpretation of the divergence of the integral for values of ξ greater than unity is that systems characterized by such values are unstable: sufficiently many counterions will ‘condense’ on the line charge to reduce ξ to a value just less than one.” (J. Chem. Phys. **51**, 924 (1969)).

Continuing, Manning argued that counterion condensation satisfactorily describes polyelectrolyte solutions up to relatively high electrolyte concentrations. This conclusion seems original to Manning, as earlier workers apparently viewed counterion condensation as a feature of salt-free solutions.

Debate

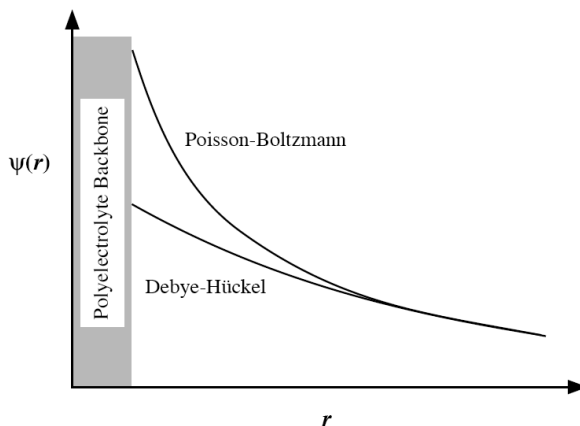
Counterion condensation has many detractors, who stress flaws in any of the concept’s derivations, such as artificial subdivision of the counterions into two populations, inappropriate extrapolation of the Debye-Hückel approximation to regions of high electrostatic potential, and inconsistent treatment of counterions. In the derivation recounted in the preceding section, for example, the electrostatic potential is calculated via the Debye-Hückel approximation, which rigorously requires linearization of all exponential Boltzmann factors, but ion distributions are subsequently evaluated using the full exponential forms of these factors. If the ion distributions are instead evaluated in their linearized forms, to maintain consistency with the Debye-Hückel approximation, the crucial divergence disappears.

The full nonlinear Poisson-Boltzmann equation offers a more rigorous way to interpret electrostatic phenomena in electrolyte solutions, but the physical picture obtained through this equation is different in many ways than the one suggested by counterion condensation. In particular, a Poisson-Boltzmann analysis does not readily identify distinct populations of condensed and free counterions but rather a Gouy-Chapman layer of smoothly varying counterion density. Nevertheless, Poisson-Boltzmann-based analyses do find that in salt-free solutions there is a fraction of counterions equal to $1-\beta$ that cannot be fully diluted away from the chain at infinite chain dilution; the volume occupied by this trapped fraction is predicted by the Poisson-Boltzmann equation to be rather large, a feature inconsistent with the physical picture on which condensation is based.

Zimm pointed out that, by applying the dilution criterion in salt-free solution to define condensed ions, all counterions are condensed on plane, none on a sphere, and some on a cylinder. Many experimental and theoretical studies support the general picture, if not the details, of the original counterion condensation concept.

Subdivision of counterions into condensed and uncondensed populations according to the Manning/Oosawa depiction is not unique. The inflection point in the radial ion distribution or the radial distance over which the electrostatic interaction energy decays to kT have both been proposed as alternative criteria for defining the condensed fraction.

According to a nonlinear Poisson-Boltzmann analysis, the initial radial decay of ψ from a cylindrical chain segment is much steeper than predicted by a Debye-Hückel analysis; see figure. The steep decay lessens at large distance, and ψ eventually adopts an asymptotic



functional form compatible with a Debye-Hückel approximation. However, to superimpose the predictions of the Poisson-Boltzmann analysis onto those formulated within the Debye-Hückel approximation, the linear charge density in the Debye-Hückel calculation must be lowered from the linear charge density asserted in the Poisson-Boltzmann analysis. The reduced, Debye-Hückel linear charge density can be interpreted, from the perspective of a distant observer, as defining the polyelectrolyte's "effective" or renormalized linear charge density, a calculation first made for linear polyelectrolytes by Fixman. The following figure compares this effective linear charge density, as determined for a charged cylinder of radius a , to the effective linear charge density predicted by the Manning line charge model with counterion condensation. The two approaches agree in only the most qualitative manner,

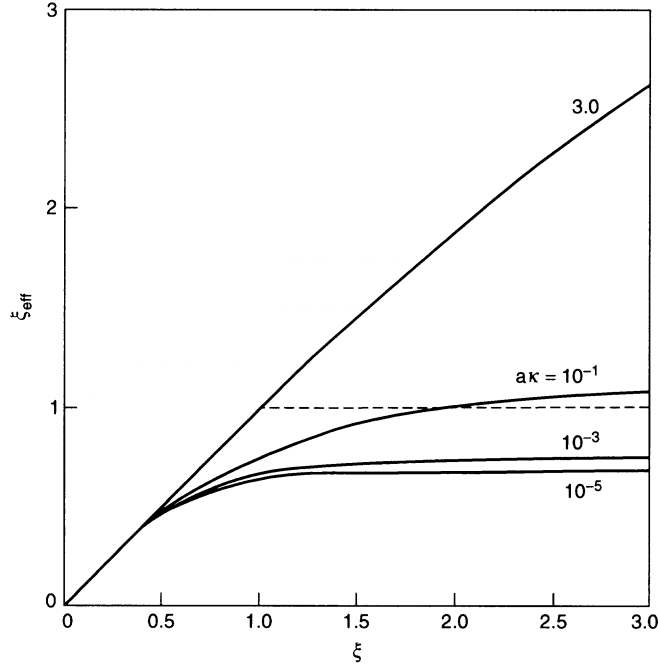


Fig. 4. Effective linear charge density ξ_{eff} of a charged cylinder derived by superimposing the far field (large r) Poisson–Boltzmann potential field onto the potential field predicted by use of the Debye–Hückel approximation. The solid lines correspond to different values of $a\kappa$, where a is the cylinder radius and κ^{-1} is the Debye length; the electrolyte is monovalent. For comparison, the counterion condensation prediction for ξ_{eff} is shown as a dotted line. Adapted from Ref. 51.

notably for $\xi \ll 1$. In this limit, where $\xi_{\text{eff}} = \xi$ according to both approaches, the Debye–Hückel approximation is valid throughout the entire solvent domain surrounding the polyelectrolyte; there are no condensed counterions. For $\xi \geq 1$, the effective linear charge and associated Debye–Hückel predictions apply only to phenomena associated with distant portions of the potential field.

Despite the unsettled theoretical status of counterion condensation, many of its predictions find direct support in experiment. Properties such as osmotic pressure, activity coefficient, and counterion diffusion coefficient can readily be understood if condensation is assumed. However, as mostly unrecognized, the same properties usually can be equally interpreted without assuming counterion condensation, albeit with the greater analytical difficulty of a Poisson–Boltzmann analysis.

The status of counterion condensation in nondilute solutions remains an active area of research; some expect the condensed fraction to rise and other for it to fall polymer concentration.

From one perspective, counterion condensation is merely a convenience. The concept enables the properties of a highly charged polyelectrolyte to be explained by a Debye–Hückel analysis when such a simplified analysis is not justified. In essence, appropriately adjusting a single parameter – the linear charge density – extends a linear theory beyond its expected linear range. The only way to verify the correctness of the overall approach is to solve the

full nonlinear problem, i.e., to develop a theory accounting quantitatively for all forces acting on counterions. Of course, with such a complete solution in hand, the need for the simplified approach disappears.

Manning expounds a slightly different view, believing that condensed counterions are not just a mathematical convenience but also a physical reality. He argues that condensed counterions form a distinct population with properties different from those of free counterions. From his perspective, counterion condensation is not – as described above – simply a way to avoid nonlinear modeling of counterions.

In support of Manning’s view, simulations by Jayaram and Beveridge (1996) strongly suggest the presence of well-defined condensed counterions around DNA, albeit the physics associated with their condensation somewhat different than those modeled by Manning. For flexible polyelectrolytes, similar simulations have been done more recently by Muthukumar and Rubenstein, and again, condensed counterions were identified.

Conformational Description –

Theories for polymer conformation often proceed at two levels, one focused at chain stiffness, expressed through the persistence length l_p , and another focused at interactions between segments widely separated along the chain contour, interactions manifested in the segmental excluded volume v . So-called “two-parameter” theories, based on the premise that the physics underlying chain conformation occur at two widely separated length scales, were originally crafted to explain the conformations of neutral polymers, a subject reviewed before turning to polyelectrolytes.

Theory of Neutral Polymer Chain Conformation:

Persistence Length –

Representing a polymer chain as a continuous but fluctuating space curve, departures from straightness can be assessed through the mean cosine of the angle θ between two backbone tangent vectors separated by curvilinear displacement Δs . In the presence of random thermal fluctuations, $\langle \cos\theta(\Delta s) \rangle$ decays exponentially with Δs , with the characteristic length of decay identified as l_p , i.e.,

$$\langle \cos\theta(\Delta s) \rangle = \exp(-\Delta s/l_p)$$

The persistence length can be interpreted as the longest chain section remaining approximately straight while the chain as a whole suffers thermal motions; upon traversing a chain section longer than l_p , bending fluctuations destroy memory of original chain direction.

The persistence length can be related to a chain’s bending modulus E by the formula,

$$l_p = E/kT$$

For an elastic chain that curves only slightly along its length L , the total bending energy U_{bend} can be obtained by integrating along the backbone,

$$U_{\text{bend}} = \frac{1}{2} E \int_0^L ds \left(\frac{\partial \mathbf{u}}{\partial s} \right)^2$$

where \mathbf{u} is the unit tangent vector to the backbone at s , and s is a curvilinear distance variable running from one chain end to the other, $0 < s < L$.

Chains with $L < 10 l_p$ are not sufficiently flexible to behave as classical flexible coils while chains with $L < l_p$ behave much as rigid rods. Chains with $l_p < L < 10 l_p$ are often described as “wormlike” chains. A formula for the mean square end-to-end distance in terms of L and l_p is written,

$$\langle R^2 \rangle_0 = 2l_p L - 2l_p^2 (1 - \exp[-L/l_p])$$

This formula, termed the Kraky-Porod formula for a persistent or wormlike chain, is general; it describes coiled ($L/l_p \gg 1$) and rod-like extremes ($L/l_p \ll 1$) as well as intermediate cases.

The formula does not account for excluded volume, which typically becomes important when L/l_p is larger than about 10-20.

Excluded Volume-

Because of chain flexibility, segments positioned far apart along the chain contour interact with one another. In this context, “far apart” implies curvilinear separations much greater than l_p . The strength of these interactions, captured in v , can dramatically affect chain conformation for a long polymer. If the interactions are attractive, the coil shrinks from its Gaussian state, and if repulsive, the coil swells from this state.

The physical interactions manifested in excluded volume are general, and the list includes van der Waals, steric, and electrostatic interactions. In most cases, the strength-distance interplay of the interactions remains poorly understood. Fortunately, detailed information is unimportant to understanding of how excluded volume impacts global chain conformation. We can simply assess the overall magnitude of the interaction through a delta function potential,

$$U(\mathbf{r}_i, \mathbf{r}_j) = v kT \delta(\mathbf{r}_i - \mathbf{r}_j)$$

where v is the segmental excluded volume (units of volume). If the full interaction potential $u(r)$ between arbitrary segment i and j is known, v can be calculated via the integral

$$v = \int d\mathbf{r} \left[1 - \exp\left(\frac{u(\mathbf{r})}{kT}\right) \right]$$

a formula analogous to that for the second virial coefficient of a nonideal gas. The integral’s form admits possibility for attractive forces over some r range to compensate exactly for repulsive forces over another r range, the compensation making v identically zero. Such a condition defines the theta temperature. When attractions among segments are sufficiently dominant, the polymer coil collapses into a globule, a transition analogous to the condensation of a gas into a liquid when molecular attractions dominate.

The subscripted “o” quantities of the previous section, obtained without concern for excluded volume, should be evaluated only at the theta temperature. When v is positive, there is an effective repulsion between distant segments, and when v is negative, there is an effective attraction. The electrostatic repulsions between like charged chain segments can increase v substantially.

The collective magnitude of excluded volume interactions depends on the instantaneous average number of segmental “collisions” within the polymer coil; this number is molecular weight-dependent. At the mean field level, the number of binary segmental interactions is of the order $N\phi$, where N is the number of polymer segments and ϕ is the volume fraction of the coil domain occupied by segments. Using a Gaussian chain description for coil volume V , the product $N\phi$ follows the scaling

$$N\left(\frac{Nv}{V}\right) \propto \frac{N^2v}{\langle R^2 \rangle^{3/2}} \propto \frac{N^2v}{N^{3/2}a^3} \propto \frac{N^{1/2}v}{a^3}$$

After attaching a numerical prefactor, the final form is traditionally termed the excluded volume strength z (a dimensionless quantity),

$$z = 2\left(\frac{3}{2\pi}\right)^{3/2} \frac{N^{1/2}v}{a^3}$$

Predicting the expansion/contraction of a chain in response to excluded volume requires a formula linking z to chain conformation. Flory, for example, proposed that

$$\alpha^5 - \alpha^3 = \frac{4}{3}z$$

where the chain expansion factor α is the ratio of the actual mean-squared end-to-end distance $\langle R^2 \rangle$ to the mean-squared end-to-end distance in the absence of excluded volume $\langle R^2 \rangle_0$,

$$\alpha^2 = \frac{\langle R^2 \rangle}{\langle R^2 \rangle_0}$$

When $z=0$, we find $\alpha=1$, defining the theta state. When z is large, $\alpha^5 \approx z$, implying

$$\langle R^2 \rangle^{1/2} \propto N^{3/5}$$

More generally, a scaling law can be written for large N ,

$$\langle R^2 \rangle^{1/2} \propto N^\mu$$

where the excluded volume exponent μ adopts values:

μ	<u>chain conformation</u>
1/3	collapsed sphere
1/2	Gaussian
3/5	self-avoiding walk
1	rod

Note that μ characterizes the molecular weight-size relationship only for asymptotically large chain lengths. When chains are not long enough to reach this limit, power law behavior is not expected, and the parameter μ should not be used. At high enough molecular weight in a good solvent, μ always equals $3/5$. (I use μ instead of the traditional Greek character ν so that there is no confusion with the Roman character ν chosen for segmental excluded volume.)

Issues for the Conformation of Charged Polymers in Solution

As reflected in size measures such as the mean radius of gyration R_g or mean-squared end-to-end distance $\langle R^2 \rangle^{1/2}$, an isolated polyelectrolyte chain in dilute solution expands relative to an analogous neutral chain because of the electrostatic repulsions among the similarly charged chain segments. Low molar mass electrolyte and counterions screen these repulsions, and consequently, a flexible polyelectrolyte contracts as electrolyte is added (assuming the electrolyte does not contain ions that specifically bind to the chain, affecting its charge in an unexpected way). In two-parameter chain descriptions, the repulsions are considered to modify l_p and ν separately.

At high enough electrolyte concentrations, suppression of segment-segment repulsions suffices, at least for some polyelectrolytes, to transform a good solvent into one of marginal or poor quality; electrostatic contributions to excluded volume are so much diminished that hydrophobic interactions between backbone segments dominate. In this case, precipitation or coacervation of the polymer ensues, a process referred to as “salting out.” Higher valence ions more effectively screen electrostatic repulsions and induce phase separation at lower salt concentrations.

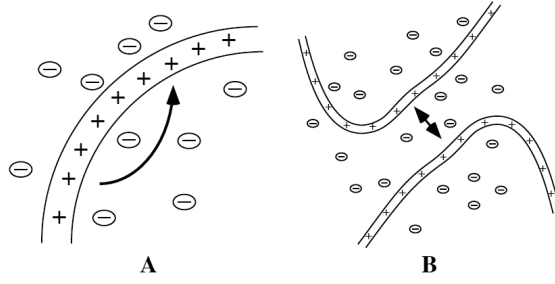
Across the ionic strength range where flexible polyelectrolytes are readily studied, 0.001 M to 1.0 M, changes in chain conformation can be significant, leading to variations of R_g of up to an order-of-magnitude.

Polyelectrolyte expansion has immediate significance to numerous solution properties such as viscosity and diffusion coefficient.

In a solution containing little added electrolyte, many early investigators expected a conformational crossover, from electrostatically stiffened rod to electrostatically swollen Flory-like coil, when chain length exceeds κ^{-1} . Later investigations showed that polyelectrolyte size and conformation in solution present subtle complexities. Although there have been important recent theoretical contributions by authors such as Odijk, Skolnick, and Fixman; Joanny and Barrat; and Muthukumar et al., the quantitative matching of experimental data to theoretical predictions remains inconclusive except in a few limiting cases.

Odijk-Skolnick-Fixman (OSF) Model

The OSF model, developed in the late 1970s by Odijk and coworkers, and independently Skolnick and Fixman, incorporates electrostatic interactions within the classical two-parameter approach.



Chain Stiffness -

The value of l_p is calculated under the approximation that a short charged chain segment undergoes only small amplitude bending deformations from its lowest energy, rod-like state. The free energy of bending ΔF is divided into two contributions, one intrinsic to the uncharged chain and the other associated with the enhancement of electrostatic interactions incurred by bending,

$$\frac{\Delta F}{kT} = \frac{l_{p,o}}{2} \int_0^L ds \left(\frac{\partial u}{\partial s} \right)^2 + \frac{\Delta F_{el}}{kT}$$

The parameter $l_{p,o}$, termed the “bare” persistence length, arises from the same local, nonelectrostatic interactions as in neutral polymers.

The term ΔF_{el} captures the electrostatic energy of bending; fixed backbone charges are brought closer together in the process of bending a previously straight chain section. For simplicity, the model assumes that fixed charges are smeared uniformly along the chain contour, and the interactions between these charges are treated at the level of the Debye-Hückel approximation. In addition, at length scales relevant to ΔF_{el} , i.e., at length scales comparable or smaller than κ^{-1} , the chain contour is assigned a mean curvature. This approximation disallows contributions to ΔF_{el} from bending fluctuations. Mathematical neglect of fluctuations requires that the bending radius of curvature must be much larger than κ^{-1} .

Retaining only the lowest, quadratic term in chain curvature, the electrostatic energy of bending can be expressed

$$\frac{\Delta F_{el}}{kT} = \frac{l_{p,e}}{2} \int_0^L ds \left(\frac{\partial u}{\partial s} \right)^2$$

where the electrostatic persistence length $l_{p,e}$ is given

$$l_{p,e} = \frac{l_b}{4} \left(\frac{1}{\kappa b} \right)^2$$

The total persistence length l_p simply sums the two contributions $l_{p,o}$ and $l_{p,e}$:

$$l_p = l_{p,o} + l_{p,e}$$

Inherent to the OSF derivation is assumption that $l_{p,e} \ll l_{p,o}$, a condition that significantly reduces the useful range of the final formula. Also, the formula does not rigorously apply to highly charged polymers, which are not properly modeled at the level of the Debye-Hückel

approximation. Nevertheless, most investigators applying the OSF result assume that the separation of l_p into intrinsic and electrostatic parts remains valid outside the theoretically justified range. Further, the phenomenon of counterion condensation is usually argued to justify the Debye-Hückel approximation, allowing OSF predictions to be applied to highly charged polyelectrolytes.

The OSF formula most importantly predicts how the electrostatic stiffness of a charged polymer depends on ionic strength I ,

$$l_{p,e} \propto I^{-1}$$

As expected, as the concentration of an added electrolyte falls, thereby lowering I , a charged chain section becomes stiffer and thus more resistant to the thermal forces that induce bending. However, experiments for inherently flexible polyelectrolytes show that the increase of $l_{p,e}$ with decreasing I more closely tracks with

$$l_{p,e} \propto I^{-1/2}$$

LeBret and Fixman polished the OSF model by adding nonlinear electrostatic effects at the level of the nonlinear Poisson-Boltzmann equation; their calculations are numerical. The figure below shows a comparison of experimental measurements with predictions of the original (Debye-Hückel) OSF model and the nonlinear OSF model (Dautzenberg et al., *Polyelectrolytes*, Hanser, 1994). The experimental data seem to fall between the two theories for the intrinsically flexible polymer examined, as shown below. (Caveat: the original OSF model curve displayed in Figure II arbitrarily assumes “counterion condensation.”)

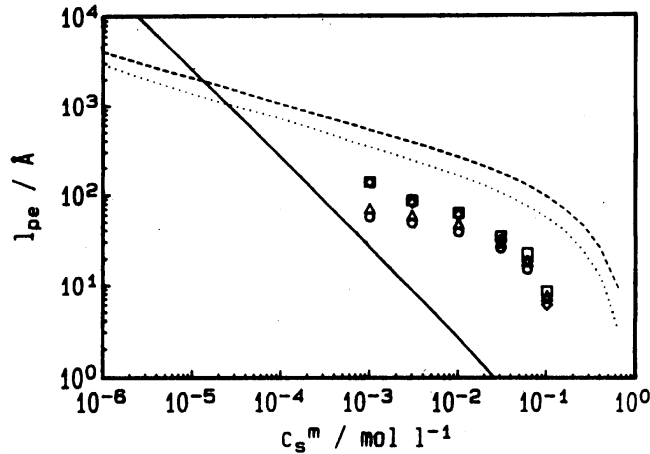


Figure 3.2 Electrostatic persistence length $l_{p,e}$ versus salt concentration. Experimental points of poly(vinylpyridiniumbenzyl bromide) in aqueous solution: (\circ) evaluated from R_H sample A, (\triangle) evaluated from R_H sample B, (\diamond) evaluated from R_G sample A, (\square) evaluated from R_G sample B. The solid line represents the OSF behavior. Numerically calculated curves are shown for $L = 8850 \text{ \AA}$ (sample A, dotted) and for $L = 22,400 \text{ \AA}$ (sample B, dashed) (with kind permission by the American Chemical Society from ref. [47]).

Analogous evaluations of the OSF model for much stiffer polymers, such as double-stranded DNA, show much better agreement between theory and experiment.

Barrat and Joanny examined the OSF model's assumptions and came to the conclusion that the model should only be applied when

$$b \ll (l_b l_{p,o})^{1/2}$$

because of its neglect of bending fluctuations. This conclusion explains why the model performs better for stiffer polymers.

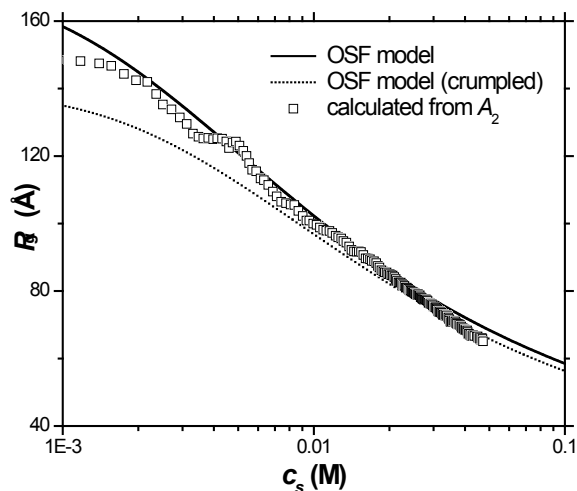
Excluded Volume -

In the OSF calculation of excluded volume, chain segments are treated as randomly oriented, charged cylinders, thereby capitalizing on Onsager's previous Debye-Hückel-level calculation of electrostatic interactions in this geometry. After averaging appropriately over segmental orientations and separations, Odijk and Houwaart found,

$$v_e = 8\pi l_p^2 \kappa^{-1}$$

as the electrostatic contribution to segmental excluded volume. Just as for persistence length, this electrostatic contribution was considered as additive to a nonelectrostatic contribution, the sum yielding the net excluded volume. Then, using the net excluded volume, chain swelling could be calculated by applying standard relationships between α and z . After these steps, one finds that at low salt, where v_e dominates, a flexible polyelectrolyte chain swells substantially beyond the ranges reached by a neutral polymer.

The following figure displays the c_s dependence of coil size (inferred by the virial coefficient measured by light scattering) for a flexible polyelectrolyte. Agreement with the OSF model is excellent, with one fitting parameter, the coil size at high c_s (Popov, Reed, and Hoagland, unpublished).



Variational Models -

Many within the polyelectrolyte community believe that variational models address the conformations of inherently flexible polyelectrolytes better than does the OSF model. In fact, the earliest models (early 1950s) were of this type, these models subsequently

overshadowed by the OSF model in the 1980s and early 1990s. Variational models have now regained their earlier stature.

In a variational approach, a flexible polyelectrolyte chain is postulated to conform to a simple physical model that constrains how the chain's conformation rearranges. Then, at each polyelectrolyte-solution condition, the model's free energy is minimized with respect to a set of model parameters (such as apparent persistence length and/or chain size), thereby obtaining a mean-field conformational description. Unlike the OSF model, changes in chain configuration are attributed to swelling in response to changes in electrostatic interactions among all segments. Local interactions, such as those corresponding to changes in persistence length within the OSF model, are not given special attention. However, the impact of electrostatic interactions on swelling may be captured in an "apparent" persistence length.

For a variational calculation, the accuracy of the final result hinges on choice of an appropriate chain model. Early studies assumed that a polyelectrolyte's segment distribution was Gaussian or that the coil remains spherical as the molecule expands or contracts from a hypothetical uncharged theta state. Modern variational models are often motivated by "blob" models that simplify analysis of electrostatic interactions.

In a variational model, the free energy is expressed as a sum of terms arising from entropic elasticity and electrostatic interaction energy, the latter most often handled at the level of the Debye-Hückel approximation.

In 1993, Barrat and Joanny motivated a variation description by depicting a weakly charged, flexible polyelectrolyte as a semiflexible string of electrostatic subunits or "blobs," each of size ξ (this symbol IS NOT the dimensionless charge density described earlier). In their model, each blob was associated with a contour section of sufficient length L' to balance electrostatic and thermal energies. Within a blob, the local chain statistics are unperturbed by electrostatic repulsions, but at larger length scales, blobs interact electrostatically and the chain becomes extended if these interactions are strong. At values of κ^{-1} appropriate to salt-free solutions, these statements lead to the following scaling forms:

Gaussian statics within a blob-

$$\xi^2 \sim L'l_o$$

Number of charges g per blob –

$$g = L' / b$$

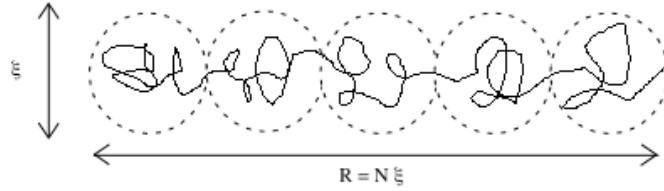
Electrostatic interactions within blob is of order kT-

$$U_e \sim kT \sim \frac{g^2 e^2}{\epsilon \xi}$$

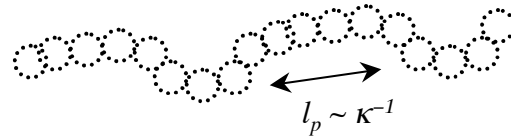
Combining these relationships, the blob size is found

$$\xi \sim (bl_o)^{2/3} l_b^{-1/3}$$

Under unscreened solution conditions, the blobs arrange linearly in space to reduce their overall electrostatic energy, as sketched below:



At finite κ^{-1} , a condition adding electrostatic screening between blobs, the depiction changes. Now, the linearity of a blob sequences is finite; this finiteness defines an apparent persistence length proportional to κ^{-1} :



When the chain of blobs is long enough, the chain obeys the usual neutral polymer scaling of R with N . From their blob depiction, Barrat and Joanny developed a variational calculation that leads to the following relationship for R at large N ,

$$R \sim N^{3/5} \kappa^{-2/5}$$

In this instance, l_p can be termed only an “apparent” electrostatic persistence length since the variational procedure self-consistently calculates both l_p and R ; obviously a close tracing of the backbone produces a persistence length much smaller than sketched.

The electrostatic blob approach fails when κ^{-1} falls below ξ .

Muthukumar et al. approached the conformation of a flexible polyelectrolyte slightly differently, employing a variational procedure that combines the Debye-Hückel approximation with the Edward’s path integral formalism. A similar formula was found for R in the limits of large and small κ^{-1} along with a crossover formula appropriate for intermediate κ^{-1} . At small values of κ^{-1} , the Muthukumar et al. formalism can be rearranged to show an apparent persistence length

$$l_p \sim \kappa^{-4/5}$$

slightly different than predicted by Barrat and Joanny.

The large κ^{-1} result of both groups corresponds to the intuitive picture that a polyelectrolyte chain unravels into an extended linear conformation when electrostatic repulsions between segments are strong. Although unraveled, the chain retains local conformational freedom and remains less than fully stretched ($R \ll L$). The large κ^{-1} formula given above for the salt-free case was actually first suggested in 1948 by Katchalsky et al. and Hermans and Overbeek and then later clarified by de Gennes et al. and Pfeuty. Similarly, the finite κ^{-1} result displayed above shows that strongly screened electrostatic repulsions between

segments can be viewed as simply increasing the chain's excluded volume. Indeed, using variational procedures, Hermans and Overbeek and Flory half a century ago derived the same small κ^{-1} formula for R; Richmond and Pfeuty more recently reported derivations.

Dobrynin et al. recently developed a variational blob theory for the dilute solution conformations of hydrophobic polyelectrolytes, those that dissolve solely only because of their charges; these polyelectrolytes were predicted to decompose into a necklace-like shape of compact beads separated by narrow strings. No experimental evidence for such shapes has surfaced.

Ionomers

(A. Eisenberg and J.-S. Kim, Introduction to Ionomers, Wiley & Sons, 1998)

Electrostatic and Morphological Description –

Electrostatics

The electrostatic and conformational descriptions of an ionomer chain are basically the same as for a polyelectrolyte. A flexible linear chain is decorated with ionizable units to extent captured in ξ (once again, this symbol represents the Manning charge parameter), defined in the same way as for a polyelectrolyte. However, the chain resides in an environment of modest or low ϵ , comprised of either similar chains (neat ionomer) or low polarity solvent molecules (ionomer solution). As a quantitative value of ϵ is usually unavailable, and since the electrostatic interactions in a dense ionomer system are not centered on a single chain or chain segment, ionizable content is more typically specified in bulk terms, for example, in mole percent of ionizable unit relative to the totally number of repeat units ($\times 100$). This content is often considered limited for ionomers to less than 15%. When the repeat units bearing ionizable units are chemically dissimilar from the unionizable or neutral repeat units, a better assessment of ionizable content is via moles per liter or milliequivalents per unit mass.

At the relevant values of ϵ and T, thermal energy is not sufficient to dissociate ionomer counterions, and so in vast preponderance, the ionizable units of an ionomer are not dissociated, instead forming “contact” ion pairs (the two ions solvated if a polar solvent is present). A very small population of dissociated ions remains present, endowing the system with a low but measurable ion conductivity. This conductivity, and strategies for raising its value, have sparked much recent research activity, motivated by applications such a fuel cell and battery membranes. Large, delocalized counterions are dissociated to somewhat greater extent than standard (small, inorganic) counterions, a principle in analogy to the strategy for creating ionic liquids.

Ion pairs attract each other due to strong dipole-dipole interactions, forming ionic aggregates. The strength of the interaction of two dipoles at contact reflects their minimal spatial separation d , a parameter altered by the sizes of both ionizable units and counterions. Making this separation dimensionless with respect to l_b defines the Coulomb coupling parameter Γ ,

$$\Gamma = \frac{l_b}{d}$$

Since ϵ is low in all ionomer environments, of the order 2-10, l_b is large, of the order 5-50 nm at room temperature. From these facts, one infers that Γ itself must be substantial, of the order 20-200.

In terms of Γ , the thermally averaged dipole-dipole interaction energy of the previous handout can be rewritten,

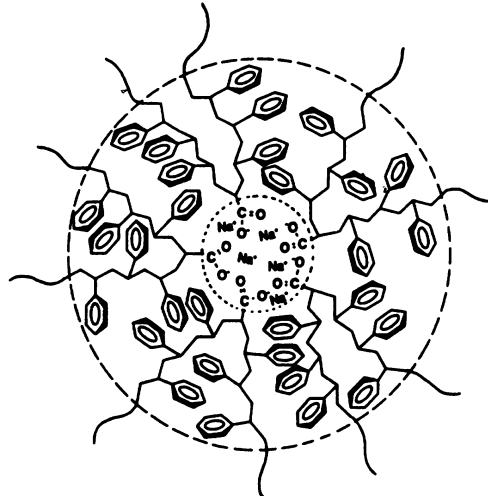
$$\frac{w(r)}{kT} = -\frac{2}{3}\Gamma^2\left(\frac{d^2l^4}{r^6}\right)$$

illustrating that Γ characterizes dipole-dipole interaction energy relative to kT . Although just a rough approximation (since the point dipole approximation has been employed and dipole-dipole energy evaluated by an orientational averaging procedure valid only for $w(r)$ small compared to kT), the strength of a contact ion pair can be estimated by setting r to d . Then,

$$\frac{w(r)}{kT} = -\frac{2}{3}\Gamma^2\left(\frac{l}{d}\right)^4$$

For the most reasonable physical situation, with d comparable to l , and with $\Gamma \gg 1$, the interaction energy is quite strong compared to kT , explaining why isolated dipoles in ionomers are rare.

Because the two positive and two negative charges adopt a preferential spatial arrangement – a square planar quartet – as two dipoles come together, a two-dipole aggregate can itself electrostatically attract other dipoles and/or dipole aggregates, thereby growing to larger size through higher order quadrupole-quadrupole and multipole-multipole interactions. The accompanying electrostatic energies, however, grow progressively weaker with size, disfavoring large aggregates. The small dipole clusters of an ionomer are called “multiplets”; they are chief morphological feature of ionomers and they will be discussed later in this handout. Multiplets are believed to be almost exclusively comprised of ion pairs, with unionizable sequences of ionomer excluded. One proposed depiction of a multiplet in sulfonated polystyrene is shown below; note the depletion of ion pairs in a shell around the multiplet (Eisenberg and Kim, Introduction to Ionomers, Wiley, 1998).



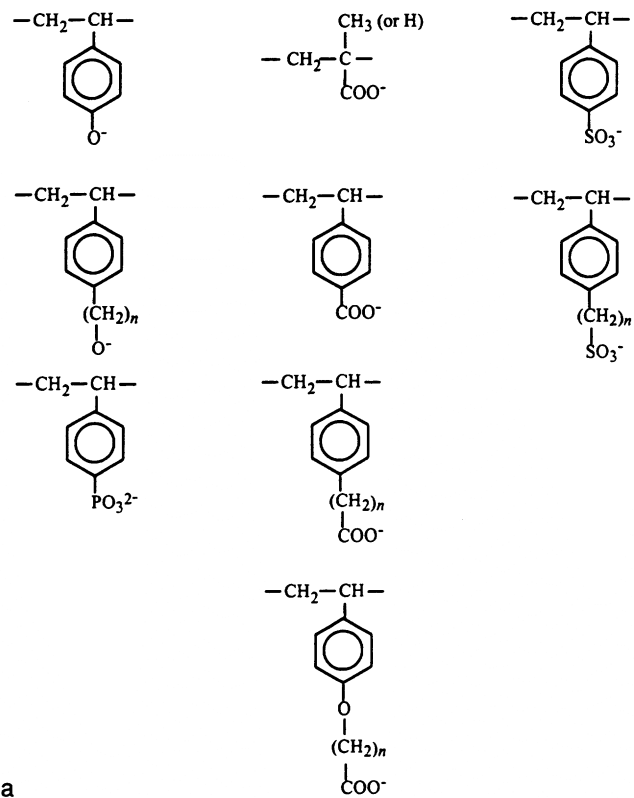
While efforts have been made to ascertain ordered arrangements among ion pairs collected in a multiplet, not much about this issue has been resolved. Some have suggested crystalline order in particular ionomer systems.

There is conflicting evidence as to the sizes of individual polymer chains in an ionomer; scattering data suggest that interacting dipoles don't much change this size in comparison to the corresponding neutral polymer.

The “neutralization” of an anionic ionomer gives the fraction of the ionizable groups that are in the salt rather than the acid form. The characteristic properties of an ionomer aren't always present in the unneutralized or acid form, presumably because the ion pairs are weakened by the small separation of charges (protons are smaller than other cations). In particular, for ionomers with carboxylate groups, multiplets are only observed in at least partially neutralized samples. In ionomers with sulfonate groups, multiplets may be observed in the completely unneutralized form, suggesting that the protonated sample shows the full range of ionomer behaviors.

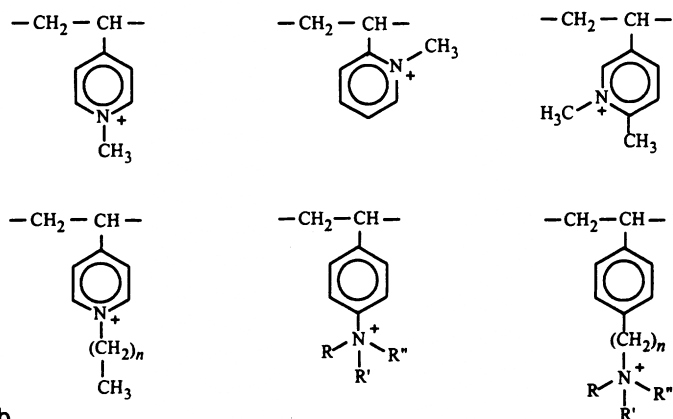
The chemistry, size, and geometry of both ionizable units and counterions are clearly more important to ionomers than to polyelectrolytes, since these features govern the interaction strength and packing of ion pairs into multiplets. Consequently, ionomers of different chemistry display distinct properties. The following tables show (i) common examples anionic and cationic ionomers and (ii) accompanying counterions (Eisenberg and Kim, Introduction to Ionomers, Wiley, 1998).

Pendent anions



a

Pendent cations



b

Figure 2.4. Examples of (a) pendent anions, mostly based on styrene, and (b) pendent cations.

Cations

Li^+ Na^+ K^+ Rb^+ Cs^+
 Mg^{2+} Ca^{2+} Sr^{2+} Ba^{2+} Zn^{2+} Ni^{2+} Mn^{2+}

Anions

F^- Cl^- Br^- I^- OTs^-

Ionizable Amines

NH_3

$\text{R}-\text{NH}_2$ $\text{RR}'-\text{NH}$ $\text{RR}'\text{R}''-\text{N}$ (R , R' or $\text{R}'' = \text{alkyl}$)

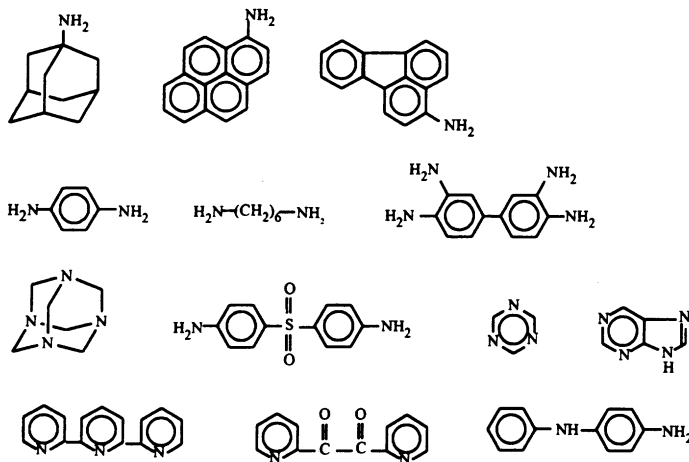


Figure 2.7. Examples of counterions. Many of the ionizable amines are described by Fan and Bazuin (80).

Morphology

Making analogy to block copolymer morphology is perhaps the simplest way to approach the nano- and micro-scale morphology of ionomers. Ionomers share many features with strongly microphase-segregated segmented block copolymers such as polyurethane elastomers, which are considered to organize into hard and soft segment domains in much the manner that ionomers organize in ionic and hydrophobic domains. The energetics governing domain separation are also much the same, and in both cases, nanoscale aggregates form highly effective physical crosslinks. Unfortunately, a successful theoretical model for multiplet formation has not been formulated, and so we proceed in our understanding of ionomer morphology by examining experimental evidence. There are strong indications that, just as in block copolymers, there are many morphological possibilities, and the one selected for a given system may depend on small details.

A distinct feature of all ionomer systems is a diffuse single “ionomer” peak in x-ray diffraction. Until recently, interpreting this peak was the chief obstacle in understanding ionomer morphology. A sample ionomer peak is given below (Yarusso and Cooper, *Macromolecules*, **16** (1983) 1871).

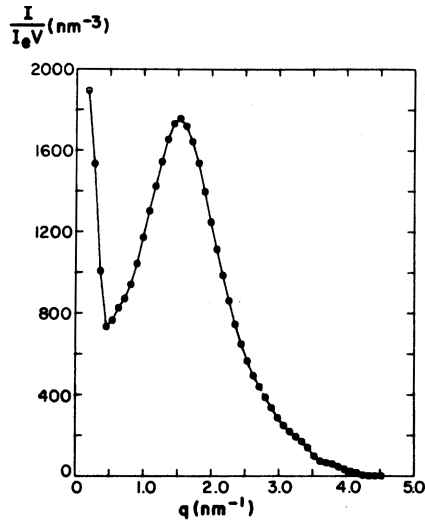


Figure 1. SAXS data for zinc-neutralized sulfonated polystyrene ionomer (sample 4D).

The Bragg spacing corresponding to the peak maximum is $\sim 2-4$ nm. Note also the upturn in intensity at still lower scattering vector, suggesting some sort of larger scale organization.

While many explanations for the ionomer peak have been offered, it is now clear that peak is explained by inter-multiplet scattering, reflecting a liquid-like spatial ordering of compact multiplets. The scattering is in all respects similar to that of hard spheres with paracrystalline or liquid-like ordering. The cited paper by Yarusso and Cooper offers a specific scattering model, depicted schematically below, which quantitatively matches the intensity profile of the scattering peak.

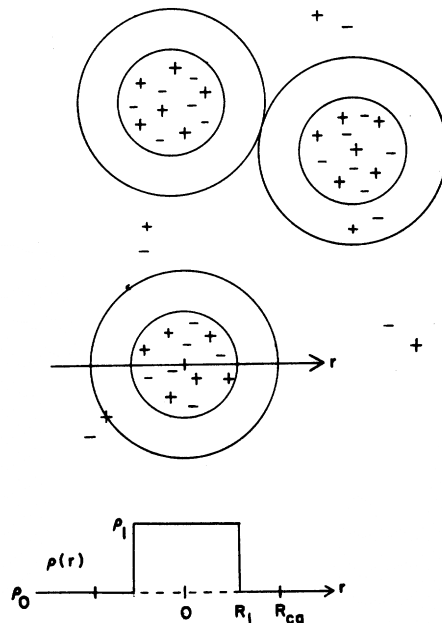


Figure 9. Schematic of modified hard-sphere model and corresponding electron density profile for one of the particles.

The key parameters are the multiplet radius (~ 1 nm), intermultiplet distance (3-4 nm), and number of ionizable units per multiplet ($\sim 15-20$); the values given in parentheses are fitted

values for zinc-neutralized sulfonated polystyrenes of various sulfonation levels and partial neutralizations with zinc. Quality of the fitted curve is shown in the next figure.

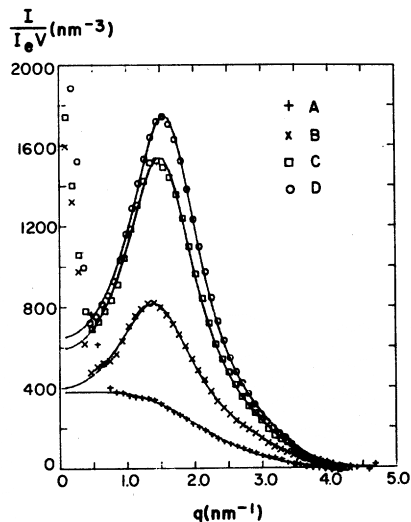


Figure 13. Fits of modified hard-sphere model (lines) to data for 85% neutralized ZnSPS (series 4) samples (symbols).

Recent support for this model comes from scanning transmission electron microscopy (STEM), which reveals multiplet structure and organization comparable to that inferred by x-ray diffraction (Winey et al., *Macromolecules* **40** (2007) 1081). The only difference is a somewhat less compact multiplet structure, containing fewer ion pairs and a compensating level of neutral chain segments. A representative STEM image is shown below (Winey et al., op. cit.).



Origins of the diffraction pattern's upturn in intensity at low q remain contentious. One possibility is a higher length scale organization of multiplets into clusters.

Nafion –

Nafion is an ionomer of unusual properties and intense technological interest. Its sulfonated ionizable units are sited at the end of short side groups attached to a perfluorinated, Teflon-like backbone. The polymer shows a typical ionomer peak and low q scattering upturn highly sensitive to uptake with water, which in technological applications as a proton-exchange membrane of a hydrogen fuel cell, is present at high levels (10-30 vol. %). For the hydrated material, a recent contribution [Schmidt-Rohr and Chen, *Nature Materials* 7 (2008) 75] makes a convincing case for a more complex morphology than conventionally ascribed to ionomers. That Nafion morphology has this added complexity is not unexpected – a percolating arrays of water transport pathways has been argued as the only explanation for its fast transport of water and protons; indeed, at 20% water, the diffusion coefficient of water in Nafion is only one order of magnitude lower than its value in bulk, and at the same time, over one order of magnitude higher than in conventional ionomers of similar water content. The proposed morphology consists of parallel, cylindrical water channels lined with the hydrophilic ionizable units, as sketched below. This model explains both the ionomer peak and the scattering upturn at low q .

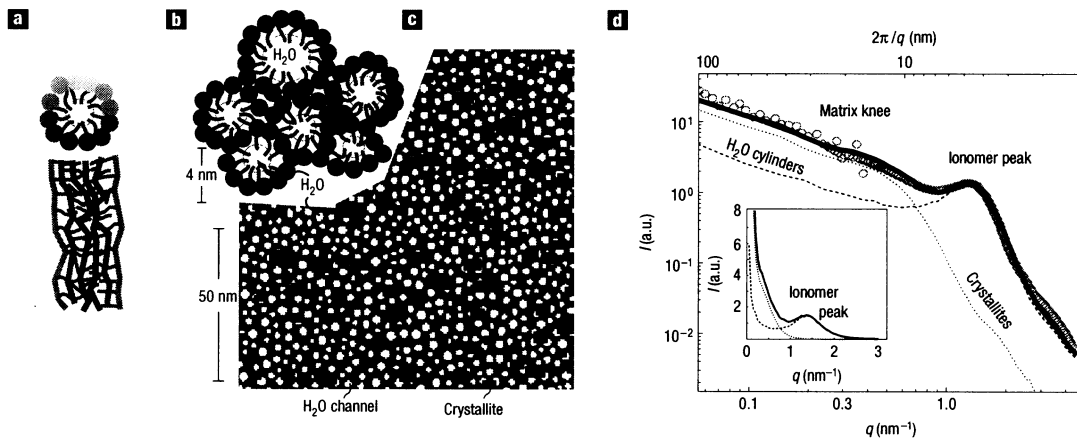


Figure 2 Parallel water-channel (inverted-micelle cylinder) model of Nafion. **a**, Two views of an inverted-micelle cylinder, with the polymer backbones on the outside and the ionic side groups lining the water channel. Shading is used to distinguish chains in front and in the back. **b**, Schematic diagram of the approximately hexagonal packing of several inverted-micelle cylinders. **c**, Cross-sections through the cylindrical water channels (white) and the Nafion crystallites (black) in the non-crystalline Nafion matrix (dark grey), as used in the simulation of the small-angle scattering curves in **d**. **d**, Small-angle scattering data (circles) of Rubatat *et al.*¹⁷ in a $\log(I)$ versus $\log(q)$ plot for Nafion at 20 vol% of H₂O, and our simulated curve from the model shown in **c** (solid line). The inset shows the ionomer peak in a linear plot of $I(q)$. Simulated scattering curves from the water channels and the crystallites by themselves (in a structureless matrix) are shown dashed and dotted, respectively.

The complexity of the suggested Nafion structure hints that, as more ionomers are explored, new and increasingly complex morphologies are likely to be discovered, a suggestion buttressed by recent simulations.